The Predictive Power of Computational Astrophysics as a Discovery Tool
Proceedings IAU Symposium No. 362, 2023
D. Bisikalo, D. Wiebe & C. Boily, eds.
doi:10.1017/S1743921322001272

Plasmoid Dominated Magnetic Reconnection and Particle Acceleration

Arghyadeep Paul[1], Sirsha Nandy[1] and Bhargav Vaidya[1]

Dept. of Astronomy Astrophysics and Space Engineering
Indian Institute of Technology Indore,
Khandwa Road, Simrol, Indore 453552, India
email: arghyadeepp@gmail.com

Abstract. The effect of a parallel velocity shear on the explosive phase of magnetic reconnection in a double tearing mode is investigated within the 2D resistive magneto-hydrodynamic framework. All the systems follow a three phase evolution pattern with the phases delayed in time for an increasing shear speed. We find that the theoretical dependence of the reconnection rate with shear remains true in more general scenarios such as that of a plasmoid dominated double current sheet system. We also find that the power-law distribution of plasmoid sizes become steeper with an increasing sub-Alfvénic shear. We further demonstrate the effect of a velocity shear on acceleration of test particles pertaining to the modification in the energy spectrum.

Keywords. Explosive reconnection, Plasmoids, Particle acceleration, Double Tearing Mode

1. Introduction

The conversion of magnetic energy to kinetic and thermal energy through the process of magnetic reconnection is ubiquitous in astrophysical and laboratory plasmas e.g, solar flares, tokamaks etc. (Mann et al. (2009), Krasheninnikov (1999)). The well known Sweet-Parker model of magnetic reconnection predicts a dependence of the reconnection rate on the Lundquist number (S) of the system as $S^{-1/2}$. This rate, however, is much slower compared to the observations from the heliophysics domain with typical high Lundquist number values. Though Petschek type reconnection improves upon the Sweet-Parker model with a weaker dependence on S, sustaining it requires localized resistivity enhancement near current sheets (Huang & Bhattacharjee (2010)). A secondary tearing instability called "plasmoid instability" occurs in a high Lundquist number ($> 10^4$) regime, which can fragment an elongated current sheet into multiple X-points, thereby facilitating a much faster magnetic reconnection with a weak dependence on Lundquist number (Daughton et al. (2006)). Multiple current sheet systems are quite prevalent in the reconnection regions (Crooker et al. (1993)) and a simplification of the same is the double tearing mode or DTM that exhibits a fast structure-driven non-linear growth phase (Janvier et al. (2011)). The dynamic nature of typical reconnection regions naturally suggests the presence of a velocity shear near the current sheets. A velocity shear flow parallel to the current sheets generally tends to throttle the growth of the tearing instability, thereby suppressing the reconnection rate. Though the relation of reconnection rate and shear speed in tearing instability (Cassak & Otto (2011)) is known to be applicable for plasmoid instability in a single current sheet (Hosseinpour et al. (2018)), the resonant flux-feedback effect of two current sheets in DTMs can affect the overall scaling of the reconnection rate with shear. Studies of particle acceleration to suprathermal energies near the reconnection regions reveal that the energy spectrum of the particles

generally follows a power law of the form $N(E) \sim E^{-1.5}$ (Drake et al. (2013)). Drake et al. (2013) have also shown that this power law is the signature of a multi-island magnetic reconnection system where the acceleration time is shorter than the loss rate of the particles, albeit the dynamics in their study were treated as non-relativistic. Akramov & Baty (2017) have also performed test particle simulations in the non-relativistic regime to study the phenomena of particle acceleration in explosive DTM reconnection with particle integration being carried out in a static fluid background. However for the study of particle acceleration in explosive reconnection phases with fast moving transient features, it is preferable to have a fluid background that evolves with the particle. In this article, we investigate the dynamics of a double current sheet system in the presence of a parallel shear flow using resistive magneto-hydrodynamic simulations in a slab geometry with emphasis on the reconnection rate and the plasmoid size distribution. We also explore the phenomena of particle acceleration in such rapidly evolving systems by introducing test particles in a moving fluid background in order to study the effect of such a shear flow from the particle energization perspective. The article is organized as follows: Section 2 describes the numerical model setup with initial conditions. Section 3 elaborates on the results of the current study and Section 4 contains the summary and some relevant additional discussions.

2. Numerical Model

Fluid setup

The numerical setup solves a set of resistive MHD equations in a 2D slab geometry using the PLUTO code (Mignone et al. (2007)). The computational domain is confined within $-L_{\rm x} \leq x \leq L_{\rm x}$ and $-L_{\rm y} \leq y \leq L_{\rm y}$ where L_x= 64.0 and L_y= 96.0 and is resolved by an uniform Cartesian grid having 1280 and 1920 grid cells along the x and y directions respectively. Since the MHD equations are scale invariant, we omit any relation of the length scales in our setup with any physical length units at this stage. Periodic boundary conditions are imposed along the x-boundaries and the y-boundaries are set to be reflective. The system is considered to be isothermal and the initial magnetic field configuration is that of a double Harris-sheet equilibrium with current sheets along $y = \pm 16$, with an asymptotic field strength $B_0 = \sqrt{2}$ and a magnetic field shear width of unity. The asymptotic Alfvén speed of the system, v_A, is defined by $B_0/\sqrt{\rho_\infty}$, and has the value $\sqrt{2}$ for our setup. Here, ρ_∞ is the density far away from the current sheet. An initial equilibrium was achieved by asserting a corresponding variation in density. An explicit resistivity was prescribed with a value of $\eta = 2 \times 10^{-5}$, which defines the corresponding Lundquist number to be, $S \sim 9 \times 10^6$. The time scale is normalised to the Alfvén transit time across the current sheet which is defined as $\tau_{\rm A} = w_B/v_{\rm A}$, where w_B is the magnetic field shear width. The in-plane velocity shear was prescribed to be of the same mathematical form as the magnetic field and the strength of the shear speed was varied from $0.0v_{\rm A}$ (no shear) to $1.0v_{\rm A}$ (Alfvénic shear) in steps of $0.25v_{\rm A}$ for this study. A small divergence-free perturbation was applied to initiate the reconnection process.

Particle Setup

To study the impact of the shear flow on the particle acceleration mechanisms in the system, we inject a total of 4 million test particles in a subset of the domain bounded by $-64 \leq x \leq 64$ and $-40 \leq y \leq 40$. To incorporate the three degrees of freedom of the particles, the domain was also extended along the z direction between $-10 \leq z \leq 10$, along which the fluid quantities are considered to be invariant. The test particles used in our setup correspond to protons with a dimensionless charge to mass ratio of unity in code units. The particles were evolved using a relativistic Boris pusher algorithm

https://doi.org/10.1017/S1743921322001272 Published online by Cambridge University Press

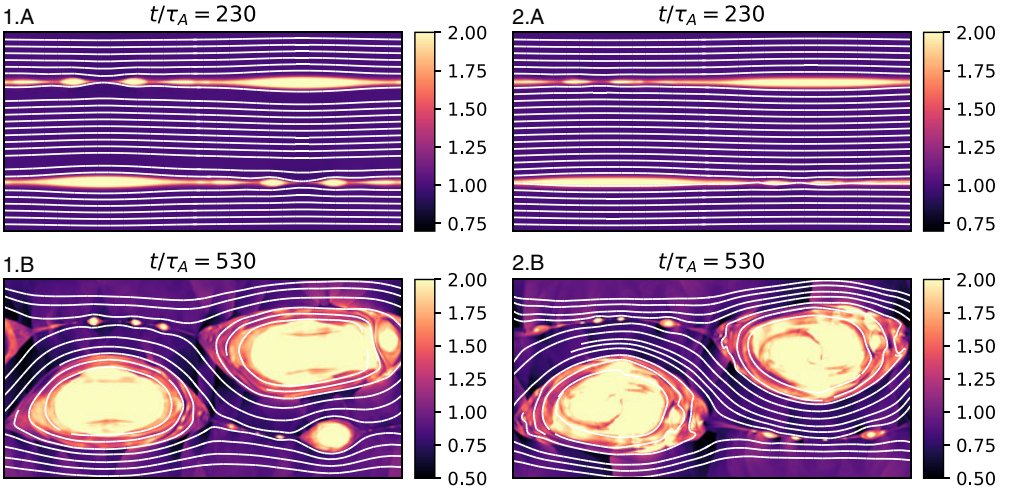

Figure 1. Figure shows the plasma density in code units over plotted by magnetic field streamlines. Figure numbers 1 and 2 (columns) correspond to a shear speed of $0.0v_{\rm A}$ and $0.50v_{\rm A}$ respectively and the labels A and B (rows) correspond to different times ($t/\tau_{\rm A} \sim 230$ and $t/\tau_{\rm A} \sim 530$).

(Mignone et al. (2018)). With the introduction of particles, the length scales are now represented in terms of $c/\omega_{\rm pi}$, which is the plasma skin depth with $\omega_{\rm pi}$ being the ion plasma frequency. The time is given in the units of the inverse cyclotron frequency $\Omega^{-1} = c/(\omega_{\rm pi} v_{\rm A})$. The particles were initialised with a gaussian distribution of velocities having a mean of zero and a standard deviation of $0.1v_{\rm A}$. An extended description of the particle setup can be found in Paul & Vaidya (2021).

3. Results

General Evolution

All the systems, irrespective of the presence of a shear flow show a similar evolution pattern with three distinct phases: (a) A slow initial growth phase, (b) A fast plasmoid dominated explosive phase and (c) A turbulent gradual relaxation phase. These phases however, are delayed in time by a certain amount with an increase in shear speed. We thus describe below the general evolution characteristics for the system with no shear as a benchmark.

During the slow growth phase ($t/\tau_{\rm A} \sim 0$ to $t/\tau_{\rm A} \sim 170$), two large islands initially form and grow. The growth rate during this phase is consistent with the wave number of the applied initial perturbation. Subsequently, the portion of the current sheets outside of the two monster islands (the secondary current sheets) start to gradually thin due to their tendency to approach a steady state Sweet-Parker inverse aspect ratio given as $\delta_{\rm SP}/L \sim S^{-0.5}$. This gradual thinning eventually fragments the current sheet into multiple small plasmoids and the system enters into the explosive plasmoid dominated fast reconnection phase. The smaller plasmoids merge into the monster plasmoids thereby increasing their size as seen from panels 1.B and 2.B of Figure 1. This increase in size enhances the coupling between the two current layers and has an effect similar to that of a coupled double tearing mode highlighted by Janvier et al. (2011). The growth rate normalised to the Alfvén transit time was calculated to be $\gamma\tau_{\rm A} \sim 4.3 \times 10^{-2}$, by fitting an exponential curve to the time evolution of the maximum value of the B_y component ($|B_y|_{max}$) during the early phases ($t/\tau_{\rm A} \sim 180$ to $t/\tau_{\rm A} \sim 220$) of the plasmoid instability.

https://doi.org/10.1017/S1743921322001272 Published online by Cambridge University Press

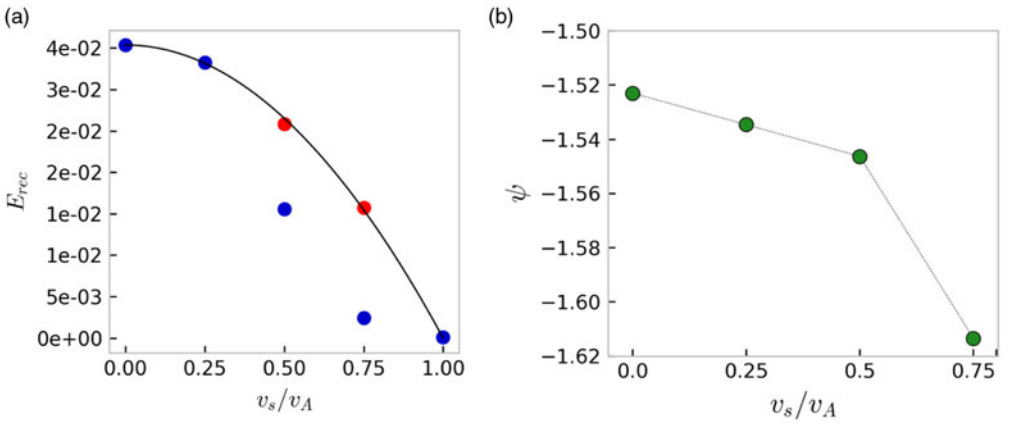

Figure 2. Panel 2(a) shows the variation of the reconnection rate with shear. The solid black line corresponds to the theoretical reconnection rate. The blue circles correspond to the reconnection rates measured during the same time interval for all the shear speeds ($t/\tau_A \sim 283$ to $t/\tau_A \sim 293$). The red circles correspond to the reconnection rates measured at different times ($t/\tau_A \sim 311$ for $v_s/v_A \sim 0.5$ and $t/\tau_A \sim 336$ for $v_s/v_A \sim 0.75$), when the island widths of all the systems are similar. Figure 2b shows the variation of the median power law indices (ψ) of the plasmoid size distribution with shear v_s/v_A.

Reconnection rate

To measure the effects of the velocity shear on the reconnection rate (E_{rec}) of the system, we measure the combined reconnection rates of the two current sheets for each system following the method given in Paul & Vaidya (2021). The reconnection rate, E_{rec} is given as the sum of the average values of the magnitude of the out of plane electric field E_z in two thin strips ($\Delta y = 2.0$) along the two current sheets. This is normalized to $B_0 v_A$ and its mathematical formulation is given below (Paul & Vaidya (2021)):

$$E_{\rm rec} = \frac{1}{B_0 v_{\rm A}} \left(\left\langle \left| \frac{\int\int_{y_1}^{y_2} E_{\rm z} dxdy}{\int\int_{y_1}^{y_2} dxdy} \right| \right\rangle + \left\langle \left| \frac{\int\int_{-y_1}^{-y_2} E_{\rm z} dxdy}{\int\int_{-y_1}^{-y_2} dxdy} \right| \right\rangle \right).$$

Here $y_1 = 15$ and $y_2 = 17$ enclosing the current sheets. Following Cassak & Otto (2011), one expects the reconnection rate to decrease with an increase in shear following the relation $E = E_0 \left(1 - \left(v_{\rm s}^2/v_{\rm A}^2\right)\right)$, where E_0 is the reconnection rate in the absence of a shear, v_s is the strength of the shear flow and v_A is the Alfvén speed of the system. We find that the system follows the theoretical scaling of the reconnection rate quite well during the early phases of the evolution before the plasmoid instability has set in (figure not shown). However, during the explosive reconnection phase (E_{rec} measured between $t/\tau_A \sim 283$ to $t/\tau_A \sim 293$), the systems with higher shear speeds deviate significantly from the theoretical scaling as seen from the blue circles in Figure 2a. The reason for this is, in a double current sheet system, the monster plasmoid of either current sheet has a feedback effect on the other wherein they tend to push magnetic flux towards the X-points of the other current sheet (Janvier et al. (2011)). Thereby, the systems with larger sized primary magnetic islands, which are the systems with a lower shear speed, experience an enhancement in the reconnection rate as seen in Figure 2a for the two systems with a shear speed of zero and $0.25 v_A$. We ascertain the above statement by measuring the reconnection rate of the systems with a shear of $0.5 v_A$ and $0.75 v_A$ when the width of the primary islands in those setups are similar to that of the setup with

https://doi.org/10.1017/S1743921322001272 Published online by Cambridge University Press

zero shear (the setups with zero and $0.25v_A$ shear have very similar island widths). This happens at $t/\tau_A \sim 311$ for $v_s/v_A \sim 0.5$ and $t/\tau_A \sim 336$ for $v_s/v_A \sim 0.75$ and the same has been plotted using red circles on Figure 2a which coincide well with the theoretical curve. This ascertains that the deviation is primarily due to the difference in the island sizes between setups with different shears which has a significant effect on the reconnection rate.

Plasmoid Size Distribution

We use the method of granulometry on the density distribution data to find the variation of the size distribution of plasmoids with an increasing shear flow. Granulometry is the application of the method of binary opening on a binary field with the mask size increasing gradually over each iteration. Before applying binary opening, the 2-dimensional plasma density data obtained from each data file saved at an interval of $1.4\tau_A$ is made binary by making use of the Otsu filter available in `python skimage` library. For our case, the mask shape is circular which calculates the equivalent radii of the plasmoids. We find that the obtained plasmoid size variation fits well with a power-law distribution $N(r) \sim r^{\psi}$, where 'r' is the equivalent radius of plasmoid. This power law distribution is consistent with simulations by Petropoulou et al. (2018) as well as observations (Patel et al. (2020)). We first fit the size distribution data for each time step to obtain the power-law index for that step. We then calculate the median of the power-law index (ψ) during a period when the variation of the index with time is nearly stationary. We repeat the whole process mentioned above for each of the four different sub-Alfvénic shear values excluding the Alfvénic shear. Figure 2b shows a decreasing trend in the values of the median power-law indices with increasing shear, indicating that the plasmoid size distribution gets steeper with an increasing shear. This suggests that as the shear speed increases, smaller plasmoids tend to be more prevalent in the system.

Particle Energy Spectrum

To investigate the energy distribution of the particles accelerated during the explosive plasmoid dominated phase, we inject test particles in a sub-domain of two setups, one with zero shear and other with a significant shear of $0.75\ v_A$. Since the explosive phase starts at different times for the two setups, the injection time is different. Therefore the energy spectrum is plotted with respect to $\Omega\Delta t'$ which denotes the duration for which the particles were integrated. We note here that the quantity $\Omega t'$ is equivalent to the fluid evolution time scale t/τ_A.

The particle energy E_{tot} is given by $0.5v_p^2$, where v_p is the particle velocity. The particle spectrum gradually evolves to form a time invariant power law distribution with a spectral index $\alpha = -1.24$, as seen from Figure 3 which shows the particle energy spectrum at three different times, namely, the early evolution phase ($\Omega\Delta t' = 68$), an intermediate stage ($\Omega\Delta t' = 109$) and the late evolution phase ($\Omega\Delta t' = 328$). The red and blue solid lines in Figure 3 correspond to the late evolution phase exhibiting the time invariant power law index. We highlight here that the presence of a shear has negligible effect on the power law index of the spectrum as seen from Figure 3 and the difference in the final time invariant spectrum of the two systems lie in the high energy tail which is truncated at lesser energies for the setup with a shear of $0.75v_A$. An inspection of the trajectories of some of the highly energized particles show that the particles accelerate in the in-plane direction as well as the out of plane direction where the in-plane energization occurs due to the interaction of the particles with fast moving transient magnetic structures in the domain, whereas, the out of plane energization is provided by the electric field which has

https://doi.org/10.1017/S1743921322001272 Published online by Cambridge University Press

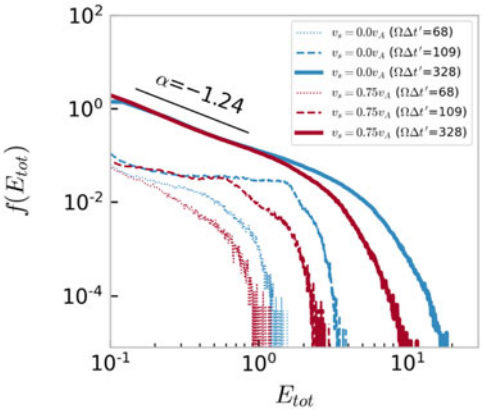

Figure 3. The normalised particle energy spectrum for the setup with zero shear (blue) and the setup with a shear of $0.75v_a$ (red) for various integration time durations. The dotted, dashed and solid lines represent time integration duration of $\Omega\Delta t' = 68$, 109 and 328 respectively.

a convective ($\mathbf{v} \times \mathbf{B}$) and a resistive ($\eta\mathbf{J}$) component. The former in-plane energization process was captured due to the fact that the particles were integrated in an evolving fluid background.

4. Summary and Discussions

We use resistive magneto-hydrodynamic simulations to examine the evolution of a high Lundquist number double current sheet system that exhibits an explosive plasmoid dominated reconnection phase. We also introduce test particles in a dynamic fluid background to investigate the phenomena of particle acceleration and the effect of the shear flow on the same. The principal highlights of the study are:

• All the systems show a three phase evolution pattern with an initial slow growth phase followed by a fast explosive reconnection phase which terminates into a gradual turbulent relaxation phase. An in-plane velocity shear generally works to suppress the tearing instability and thus, the second and the third phases are delayed in time by a certain amount with an increase in the shear flow magnitude.

• The reconnection rate obtained during the early phases is well in agreement with the theoretical values. During the later stages however, the reconnection rate agrees with the theoretical values only when the rates are measured at different times when the size of the primary magnetic islands (monster plasmoids) are similar. This shows that the variation of size of the primary magnetic islands must be taken into account while determining the scaling of the reconnection rate.

• The plasmoid size distribution is obtained using the granulometry technique. We found that the plasmoid size distribution fits well with a power law distribution. We also found that the median power law index ψ for the setups with different sub-Alfvénic shears lies within a range of -1.61 to -1.52 and has a decreasing trend with an increase in the magnitude of shear. This indicates that smaller plasmoids are more prevalent in setups with higher shear speed.

• The energy spectrum of the accelerated particles also eventually attains a time invariant power law distribution with a spectral index of -1.24. The presence of a shear flow has negligible effect on the spectral index of the particles. However, the presence of a shear flow does make the overall acceleration process less efficient (see Paul & Vaidya (2021) for details), which results in a truncation of the high energy portion of the spectrum at a lower value.

https://doi.org/10.1017/S1743921322001272 Published online by Cambridge University Press

In this study, however, we have not considered the effect of a guide field which can have significant effects on the particle acceleration due to ion heating. This study also considers the ions as test particles meaning that they do not provide any feedback to the fluid. As a natural extension of this study, the effect of the particle feedback, wherein, the motion of the particles deposits fields back to the grid, would be an interesting future prospect.

References

Paul, A. & Vaidya, B. 2021, Physics of Plasmas, 28, 082903. doi:10.1063/5.0054501
Mignone, A., Bodo, G., Massaglia, S., et al. 2007, apjs, 170, 228. doi:10.1086/513316
Mignone, A., Bodo, G., Vaidya, B., et al. 2018, apj, 859, 13. doi:10.3847/1538-4357/aabccd
Janvier, M., Kishimoto, Y., & Li, J. Q. 2011, prl, 107, 195001. doi:10.1103/PhysRevLett.107.195001
Cassak, P. A. & Otto, A. 2011, Physics of Plasmas, 18, 074501. doi:10.1063/1.3609771
Patel, R., Pant, V., Chandrashekhar, K., et al. 2020, aap, 644, A158. doi:10.1051/0004-6361/202039000
Petropoulou, M., Christie, I. M., Sironi, L., et al. 2018, mnras, 475, 3797. doi:10.1093/mnras/sty033
Hosseinpour, M., Chen, Y., & Zenitani, S. 2018, Physics of Plasmas, 25, 102117. doi:10.1063/1.5061818
Drake, J. F., Swisdak, M., & Fermo, R. 2013, apjl, 763, L5. doi:10.1088/2041-8205/763/1/L5
Akramov, T. & Baty, H. 2017, Physics of Plasmas, 24, 082116. doi:10.1063/1.5000273
Huang, Y.-M. & Bhattacharjee, A. 2010, Physics of Plasmas, 17, 062104. doi:10.1063/1.3420208
Daughton, W., Scudder, J., & Karimabadi, H. 2006, Physics of Plasmas, 13, 072101. doi:10.1063/1.2218817
Crooker, N. U., Siscoe, G. L., Shodhan, S., et al. 1993, jgr, 98, 9371. doi:10.1029/93JA00636
Mann, G., Warmuth, A., & Aurass, H. 2009, aap, 494, 669. doi:10.1051/0004-6361:200810099
Krasheninnikov, S. I. 1999, APS Division of Plasma Physics Meeting Abstracts

5. Questions and Answers

Q1. There have been studies of particle acceleration in the presence of velocity gradients without considering reconnection where the particles accelerate in some kind of Fermi mechanisms. Do you see any of that in your setup?

Ans: In our setup, the acceleration was actually due to a combined effect of electric fields and Fermi mechanisms. It is difficult to isolate the particle energization that occurs solely due to the velocity gradient.

Q2. How complex would it be to set up your code in different geometries? You gave some examples of Cartesian meshing but are you able to adapt the geometry of your code to the problem that you want to treat?

Ans: The simulations that we did were solved using the MHD code PLUTO which has this hybrid MHD-PIC framework. All the simulations that I discussed are indeed done in Cartesian coordinates because the particle module in PLUTO code currently only supports the Cartesian geometry for now. Maybe in the future we will be able to address different geometries.